Boundary-Layer Meteorol (2011) 140:411–428
DOI 10.1007/s10546-011-9621-5

ARTICLE

A Comprehensive Modelling Approach for the Neutral Atmospheric Boundary Layer: Consistent Inflow Conditions, Wall Function and Turbulence Model

Alessandro Parente · Catherine Gorlé · Jeroen van Beeck · Carlo Benocci

Received: 10 July 2010 / Accepted: 5 May 2011 / Published online: 26 May 2011

Abstract We report on a novel approach for the Reynolds-averaged Navier-Stokes (RANS) modelling of the neutral atmospheric boundary layer (ABL), using the standard k–ε turbulence model. A new inlet condition for turbulent kinetic energy is analytically derived from the solution of the k–ε model transport equations, resulting in a consistent set of fully developed inlet conditions for the neutral ABL. A modification of the standard k–ε model is also employed to ensure consistency between the inlet conditions and the turbulence model. In particular, the turbulence model constant C_μ is generalized as a location-dependent parameter, and a source term is introduced in the transport equation for the turbulent dissipation rate. The application of the proposed methodology to cases involving obstacles in the flow is made possible through the implementation of an algorithm, which automatically switches the turbulence model formulation when going from the region where the ABL is undisturbed to the region directly affected by the building. Finally, the model is completed with a slightly modified version of the Richards and Hoxey rough-wall boundary condition. The methodology is implemented and tested in the commercial code Ansys Fluent 12.1. Results are presented for a neutral boundary layer over flat terrain and for the flow around a single building immersed in an ABL.

A. Parente (✉)
Service d'Aéro-Thermo-Mécanique, Université Libre de Bruxelles, Avenue F. D. Roosevelt 50, 1050 Bruxelles, Belgium
e-mail: Alessandro.Parente@ulb.ac.be

A. Parente · J. van Beeck · C. Benocci
Environmental and Applied Fluid Dynamic Department, Von Karman Institute for Fluid Dynamics, Bruxelles, Belgium

C. Gorlé
Center for Turbulence Research, Stanford University, Stanford, CA, USA

C. Gorlé
Department of Physics, University of Antwerp, EMAT, Antwerp, Belgium

Keywords Fully-developed inlet profiles · k–ε turbulence model · Neutral atmospheric boundary layer · Rough-wall function

1 Introduction

There is an increasing interest in the application of computational fluid dynamics (CFD) to study flow phenomena in the lower part of the atmospheric boundary layer (ABL). Numerical simulations of ABL flows can be performed either by solving the Reynolds-averaged Navier-Stokes (RANS) equations or by conducting large-eddy simulations (LES). It is generally acknowledged that LES, which explicitly accounts for the larger spatial and temporal turbulent scales, can provide a more accurate solution for the turbulent flow field, provided that the range of resolved turbulent scales is sufficiently large and that the inflow conditions are well characterized (Shah and Ferziger 1997; Xie and Castro 2006; Lim et al. 2009). For example, Xie and Castro (2006) presented a comparison of LES and RANS for the flow over an array of uniform height wall-mounted obstacles: the authors compared the results to available direct numerical simulation (DNS) data, showing the superior performances of LES within the canopy. Dejoan et al. (2010) compared LES and RANS for the simulation of pollutant dispersion and found that LES better predicted vertical velocity and Reynolds shear stress, whereas the results for streamwise velocity were comparable.

However, LES simulations are at least one order of magnitude computationally more expensive than RANS (Rodi 1997). Moreover, the sensitivity of LES to input parameters such as the boundary conditions implies that, likewise RANS, multiple simulations are needed to quantify the uncertainty in the results. Hence, practical simulations of ABL flows are still often carried out using RANS in combination with two-equation turbulence models. Consequently, investigating possible improvements to these models is still worthwhile.

In RANS simulations, the effect of surface roughness is generally represented with the so-called sand-grain wall functions (Cebeci and Bradshaw 1977), based on the experiments conducted by Nikuradse (1933) for flow in rough, circular pipes covered with sand. Moreover, the upstream turbulent characteristics of a homogeneous ABL flow are often modelled using the profiles suggested by Richards and Hoxey (1993) for mean velocity, turbulent kinetic energy and turbulent dissipation rate.

However, this modelling approach can result in an unsatisfactory reproduction of the ABL for two main reasons. The first cause of discrepancy lies in the inconsistency between the fully-developed ABL inlet profiles and the rough-wall function formulation (Riddle et al. 2004; Franke et al. 2004, 2007; Blocken et al. 2007a,b; Hargreaves and Wright 2007). Furthermore, the inlet profile for the turbulence kinetic energy, k, proposed by Richards and Hoxey (1993), assumes a constant value with height, in conflict with wind-tunnel measurements (Leitl 1998; Xie et al. 2004; Yang et al. 2009), where a variation of k with height is observed.

A remedial measure to solve the inconsistency between the sand-grain based rough-wall function and the fully-developed inlet profiles was proposed by Blocken et al. (2007b). It consists in the modification of the wall-law coefficients, namely the equivalent sand-grain roughness height k_s and the roughness constant C_s, to ensure a proper matching with the velocity boundary conditions. This approach ensures the desired homogeneity of the velocity distribution in the streamwise direction, but it is code dependent and does not provide a general solution to the problem. Moreover, the standard law of the wall for rough surfaces poses limitations concerning the level of grid refinement that can be achieved at the wall. This restriction becomes particularly relevant for applications requiring a high resolution

near the wall boundaries. An additional complicating factor is the necessity to apply different wall treatments when a combination of rough terrains and smooth building walls must be simulated.

Concerning the inlet profile for turbulent kinetic energy, Yang et al. (2009) derived a new set of inlet conditions, with k decreasing with height. However, the application of such a profile at the inlet boundary only provides an approximate solution for the system of equations describing a fully-developed ABL. Recently, Gorlé et al. (2009) proposed a modification of the constant C_μ and of the turbulent dissipation Prandtl number, σ_ε, to ensure homogeneity along the longitudinal ABL direction, when the k profile of Yang et al. (2009) is applied.

Parente and Benocci (2010) and Parente et al. (2011) proposed a modification of the k–ε turbulence model compatible with the set of inlet conditions proposed by Yang et al. (2009). Such a modification consisted in the generalization of the model coefficient C_μ, which becomes a local function of the flow variables, and in the introduction of two source terms in the transport equations for k and ε, respectively. The limitation of such an approach consisted in the inlet profile adopted for turbulent kinetic energy, which does not satisfy all the governing equations involved in the problem (Parente et al. 2011).

The present article addresses the aforementioned aspects and proposes a comprehensive approach for the numerical simulation of the neutral ABL. First, a new profile for turbulent kinetic energy is derived from the solution of the turbulent kinetic energy transport equation, resulting in a new set of fully-developed inlet conditions for the neutral ABL. The consistency between the inlet profiles and the standard k–ε model is ensured with the introduction of a universal source term in the transport equation for the turbulent dissipation rate, ε, and the re-definition of the k–ε model coefficient C_μ as a location-dependent parameter. Second, for the purpose of solving the flow around obstacles immersed in the flow, the approach derived for the homogeneous ABL is generalized with an algorithm for the automatic identification of the building influence area (BIA). As a consequence, the turbulence model formulation is gradually adapted moving from the undisturbed ABL (Sect. 2.1) to the region affected by the obstacle (Sect. 2.3).

The approach is completed by the implementation of a wall function, which incorporates both smooth- and rough-wall treatments (Sect. 2.2). A screening algorithm is employed to automatically select the desired formulation, i.e. rough or smooth, depending on the boundary surface properties. Interestingly, the rough-wall treatment is not based on the sand-grain equivalent roughness parameters but depends directly on the aerodynamic roughness, as prescribed by Richards and Hoxey (1993).

The methodology is first validated for the simple case of a neutral ABL over flat terrain. Then, the simulation of the flow around a ground-mounted bluff body is carried out to investigate the applicability of the approach to cases involving obstacles immersed in the ABL and separated flows. The proposed approach is implemented and tested in the commercial code Ansys Fluent 12.1 by Ansys Inc., by means of user-defined functions, available upon request.

2 Theory

The standard k–ε model remains the most popular modelling approach for the numerical simulation of ABL flows. Assuming a steady, incompressible and horizontally homogenous flow, a two-dimensional ABL can be described by the following equations for momentum, turbulent kinetic energy, k, and turbulent dissipation rate, ε (Richards and Hoxey 1993):

$$\mu_T \frac{\partial u}{\partial z} = \tau_w = \rho u_*^2, \tag{1}$$

$$\frac{\partial}{\partial_z}\left(\frac{\mu_t}{\sigma_k}\frac{\partial_k}{\partial_z}\right) + G_k - \rho\varepsilon = 0, \tag{2}$$

$$\frac{\partial}{\partial_z}\left(\frac{\mu_t}{\sigma_\varepsilon}\frac{\partial_\varepsilon}{\partial_z}\right) + C_{\varepsilon 1} G_k \frac{\varepsilon}{k} - C_{\varepsilon 2}\rho\frac{\varepsilon^2}{k} = 0, \tag{3}$$

where u is the longitudinal velocity component, ρ is the density of the fluid, τ_w is the wall-shear stress, $u_* = (\tau_w/\rho)^{0.5}$ is the friction velocity and G_k is the production of turbulent kinetic energy, $G_k = \mu_t\,(\partial u/\partial z)^2$. Equations (1–3) have been written under the hypothesis of highly turbulent flows, i.e. assuming the molecular viscosity, μ, is negligible with respect to the turbulent viscosity, μ_t

$$\mu_t = \rho C_\mu \frac{k^2}{\varepsilon}. \tag{4}$$

In Eqs. (2) and (3), σ_k, σ_ε, $C_{\varepsilon 1}$, $C_{\varepsilon 2}$ and C_μ are coefficients of the k–ε turbulence model.

2.1 Inlet Conditions and Turbulence Model

Fully-developed inlet profiles of mean velocity, turbulent kinetic energy and dissipation rate under neutral stratification conditions are often specified following Richards and Hoxey (1993):

$$u = \frac{u_*}{k}\mathrm{In}\left(\frac{z+z_0}{z_0}\right), \tag{5}$$

$$k = \frac{u_*^2}{\sqrt{C_\mu}}, \tag{6}$$

$$\varepsilon = \frac{u_*^3}{k\,(z+z_0)}, \tag{7}$$

where κ is the von Karman constant and z_0 is the aerodynamic roughness length. It can be shown that Eqs. (5–7) are analytical solutions of the standard k–ε model if the turbulent dissipation Prandtl number, σ_ε, is defined as $\sigma_\varepsilon = k^2/\left(C_{\varepsilon 2} - C_{\varepsilon 1}\right)\sqrt{C_\mu}$ (Richards and Hoxey 1993), or, equivalently (Pontiggia et al. 2009; Parente et al. 2011), if the following source term is added to the dissipation rate equation:

$$S_\varepsilon\,(z) = \frac{\rho u_*^4}{(z+z_0)^2}\left(\frac{\left(C_{\varepsilon 2} - C_{\varepsilon 1}\right)\sqrt{C_\mu}}{k^2} - \frac{1}{\sigma_\varepsilon}\right). \tag{8}$$

A weakness of the formulation presented above is the assumption of a constant value for the turbulent kinetic energy k in Eq. (6). Indeed, experimental observations show a decay of k with height (Leitl 1998; Xie et al. 2004; Yang et al. 2009). Following this observation, Yang et al. (2009) analytically derived an alternative inlet condition for k:

$$k\,(z) = \sqrt{C_1 \mathrm{In}\,(z+z_0) + C_2} \tag{9}$$

where C_1 and C_2 are constants determined via experimental data fitting. The profile for k expressed by Eq. (9) is directly obtained as a solution of the turbulent kinetic energy transport equation, under the assumption of a constant C_μ and local equilibrium between production and dissipation:

$$\varepsilon(z) = \sqrt{C_\mu} k \frac{\partial u}{\partial z}. \tag{10}$$

Yang et al. (2009) mentioned that C_μ had be properly specified in order to ensure the correct level of turbulence kinetic energy throughout the domain. Gorlé et al. (2009) investigated the effect of a non-constant k profile on the momentum equation, obtaining the following relation between C_μ and k, by substituting Eqs. (4) and (10) in Eq. (1):

$$C_\mu(z) = \frac{u_*^4}{k(z)^2}. \tag{11}$$

However, a closed expression of σ_ε satisfying Eqs. (1–3) could not be found when employing Eq. (11) for C_μ. Therefore, an approximate solution for σ_ε was derived, using the constant value of C_μ obtained at the wall adjacent cell. Parente et al. (2011) proposed an improved k–ε turbulence model for the neutral ABL, through the generalization of the coefficient C_μ according to Eq. (11) and the introduction of an additional source term for the k transport equation, $S_k = (\rho u_* k/\sigma_k)\, \partial\left[(z + z_0)\, \partial k/\partial z\right]/\partial z$, in addition to the one expressed by Eq. (8) for the ε transport equation. As a consequence, an arbitrary set of inlet conditions, including the ones of Yang et al. (2009), could be adopted at the inlet boundary, ensuring their conservation throughout the computational domain.

In the present study, the generalization of the coefficient C_μ according to Eq. (11) is the starting point for the derivation of a new, consistent inlet profile for turbulent kinetic energy. In particular, assuming local equilibrium between turbulence production and dissipation (Eq. 10), Eq. (2) can be simplified to:

$$\frac{\partial}{\partial_z}\left(\frac{\mu_t}{\sigma_k}\frac{\partial k}{\partial z}\right) = 0. \tag{12}$$

Substituting Eqs. (4), (10) and (11) into Eq. (12) and employing the analytical derivative of the logarithmic velocity profile, the following expression is obtained:

$$\frac{\partial}{\partial z}\left(\frac{1}{\sigma_k}\rho C_\mu \frac{k^2}{\sqrt{C_\mu} k \frac{\mathrm{d}u}{\mathrm{d}z}}\frac{\partial k}{\partial z}\right) = \frac{\partial}{\partial z}\left(\frac{k\rho u_*}{\sigma_k}(z + z_0)\frac{\partial k}{\partial z}\right) = 0 \tag{13}$$

which gives:

$$(z + z_0)\frac{\partial k}{\partial z} = \text{const}. \tag{14}$$

By integrating Eq. (14), the following general solution for turbulent kinetic energy profile is derived:

$$k(z) = C_1 \mathrm{In}(z + z_0) + C_2, \tag{15}$$

which differs from Eq. (9) since the square root disappears. Similarly to Eq. (9), C_1 and C_2 are constants determined by fitting the equations to the measured profile of k.

Concerning the profile of turbulent dissipation rate, the equilibrium assumption (Eq. 10) and the generalization of C_μ (Eq. 11) ensure that Eq. (7) remains valid also for a kinetic energy profile given by Eq. (15). The full set of inlet conditions, the turbulence model formulation and the wall-function implementation are summarized in Table 1. The set of inlet boundary conditions provided by Eqs. (5), (15) and (7) for velocity, turbulent kinetic energy and dissipation rate, respectively, represents a consistent extension of the formulation proposed by Richards and Hoxey (1993) to the case of a non-constant turbulent kinetic energy

Table 1 Inlet conditions, turbulence model and wall-function formulation

Inlet conditions	$u\,(z)$	Eq. (5)
	$k\,(z)$	Eq. (15)
	$\varepsilon\,(z)$	Eq. (7)
Turbulence model	μ_t	Eq. (4)
	$S_\varepsilon\,(z)$	Eq. (8)
	$C_\mu\,(z)$	Eq. (11)
Wall function $u = \frac{u_*}{k}\ln\left(E' z^{+\prime}\right)$	u_*	$C_\mu^{0.25} k_p^{0.5}$
	E', $z^{+\prime}$	Eq. (17)

profile. Indeed, if Eq. (15) for k and Eq. (11) for C_μ are used, the transport equation for the turbulent dissipation rate is identically satisfied by the source term S_ε (Eq. 8), which is independent of the specific form of the inlet profile. In fact, the equilibrium assumption and the generalization of the coefficient C_μ make the first term of Eq. (3) universal and equal to:

$$\frac{\partial}{\partial z}\left(\frac{\mu_t}{\sigma_\varepsilon}\frac{\partial \varepsilon}{\partial z}\right) = \frac{\partial}{\partial z}\left(\frac{\rho C_\mu}{\sigma_\varepsilon}\frac{k^2}{\sqrt{C_\mu}k\frac{\mathrm{d}u}{\mathrm{d}z}}\frac{\partial \sqrt{C_\mu}k\frac{\mathrm{d}u}{\mathrm{d}z}}{\mathrm{d}z}\right) = \frac{\rho u_*^4}{\sigma_\varepsilon (z+z_0)}. \tag{16}$$

Moreover, it can be observed that, assuming a constant profile for k, i.e. $C_1 = 0$ in Eq. (15), the proposed approach reduces to a formulation equivalent to the one proposed by Richards and Hoxey (1993), with the difference that the proper value of C_μ is automatically selected via Eq. (11).

2.2 Wall Treatment

In order to overcome the limitations of the standard rough-wall functions, a formulation based on the aerodynamic roughness was adopted, following Parente et al. (2011). In particular, velocity and turbulent dissipation rate are fixed at the first cell centroid, z_p, as in Richards and Hoxey (1993), i.e. $u = (u_*/k)\ln\left[(z_p + z_0)/z_0\right]$ and $\varepsilon_w = \left(C_\mu^{0.75} k^{105}\right)/\left[k\,(z_p + z_0)\right]$. Differently from Richards and Hoxey (1993), the production of turbulent kinetic energy at the wall, $G_k = \tau_w^2/\left[\rho k C_\mu^{0.25} k^{0.5}\,(z_p + z_0)\right]$, is not integrated over the first cell height but computed at $(z_p + z_0)$. This formulation was verified (Parente et al. 2011) to avoid the well-documented peak of turbulent kinetic energy at the wall (Hargreaves and Wright 2007; Norris and Richards 2010). The wall function allows both smooth- and rough-wall treatments. In particular, the law of the wall is expressed in terms of non-dimensional parameters as $u = (u_*/k)\ln\left(E' z^{+\prime}\right)$, where E' and $z^+$are defined as:

$$E' = \begin{cases} E & \text{smooth} \\ \frac{v}{z_0 u_*} & \text{rough} \end{cases} \quad z' = \begin{cases} \frac{z_p u_*}{v} & \text{smooth} \\ \frac{(z_p + z_0) u_*}{v} & \text{rough} \end{cases} \tag{17}$$

In Eq. (17) the friction velocity, u_*, is not kept constant in the longitudinal direction but calculated as $u_* = C_\mu^{0.25} k_p^{0.5}$. The described approach removes the drawbacks of the standard wall function, without reducing its flexibility: the implementation is, in fact, based on a screening algorithm, which retrieves the roughness properties for each boundary and sets the parameters E' and $z^{+\prime}$ accordingly.

2.3 Generalization of the ABL Model for the Case of Obstacles Immersed in the Flow

The methodology developed for the neutral ABL in Sect. 2.1 is valid when the ABL is undisturbed. When an obstacle is immersed in the flow field, the relations derived for the turbulence model parameter C_μ (Eq. 11) and the turbulent dissipation rate source term S_ε (Eq. 8) are no longer valid, since the governing equations are no longer given by Eqs. (1–3). Following these considerations, Gorlé et al. (2010) proposed a modification of the turbulence model parameters C_μ and σ_ε in a building influence area (BIA), defined (Beranek 1979) as a half sphere with radius $r = 1.6H$, centred $0.16H$ downstream of the building, H being the building height. Parente et al. (2011) further investigated the effect of the BIA size and shape, indicating the need for more advanced models able to automatically determine the BIA during the numerical simulations.

The present article proposes an approach allowing a gradual transition from the formulation proposed for the undisturbed ABL to one more appropriate for the wake-flow region. A local deviation from the undisturbed ABL conditions is introduced, which automatically identifies the extent of the flow region affected by the obstacle. The deviation, δ, of the actual local velocity profile, u, with respect to the inlet logarithmic profile, $u_{\log,\mathrm{ABL}}$, is taken as the blending parameter:

$$\delta = \min\left[\left(\frac{u - u_{\log,\mathrm{ABL}}}{u_{\log,\mathrm{ABL}}}\right), 1\right]. \tag{18}$$

The coefficient C_μ and the source term S_ε are then weighted as a function of δ, to allow a gradual transition between different flow regions:

$$\phi = \phi_{\mathrm{std}} + \left(1 - \delta^\alpha\right)\left(\phi_{\mathrm{hom}} - \phi_{\mathrm{std}}\right) \tag{19}$$

where ϕ indicates S_ε or C_μ, the subscript hom indicates the value of the parameters for a homogeneous ABL (Eqs. 8 and 11), whereas std refers to the standard k–ε model values, $S_\varepsilon = 0$ and $C_\mu = 0.09$. The parameter α determines the shape of the transition function between the different formulations. Different values of α have been tested, as will be discussed in Sect. 3.2.

3 Test Cases

The proposed methodology is first presented for a neutral ABL over flat terrain. Then, the flow around a ground-mounted bluff body is modelled, to investigate the performance of the approach for the simulation of the flow around urban obstacles. For both cases, the Ansys Fluent 12.1 steady, double precision, pressure-based solver was used. Second-order schemes were adopted for momentum and turbulence quantities and the SIMPLE approach was selected for the pressure–velocity coupling. The simulations were run until the residuals for all the resolved quantities levelled out, resulting in a decrease of at least six orders of magnitude. In addition flow field variables at different locations were monitored to check convergence to the steady state solution.

3.1 Neutral ABL Over Flat Terrain

A neutral ABL over flat terrain was simulated at wind-tunnel scale using a two-dimensional domain of 4 m length and 1 m height (Fig. 1), for which velocity and turbulence intensity measurements are available (CEDVAL A1-1) (Leitl 1998) (Fig. 2).

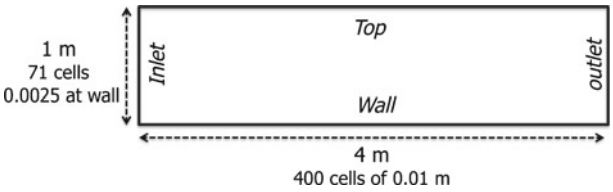

Fig. 1 Schematic of the computational domain adopted for the numerical simulation of the neutral ABL over flat terrain

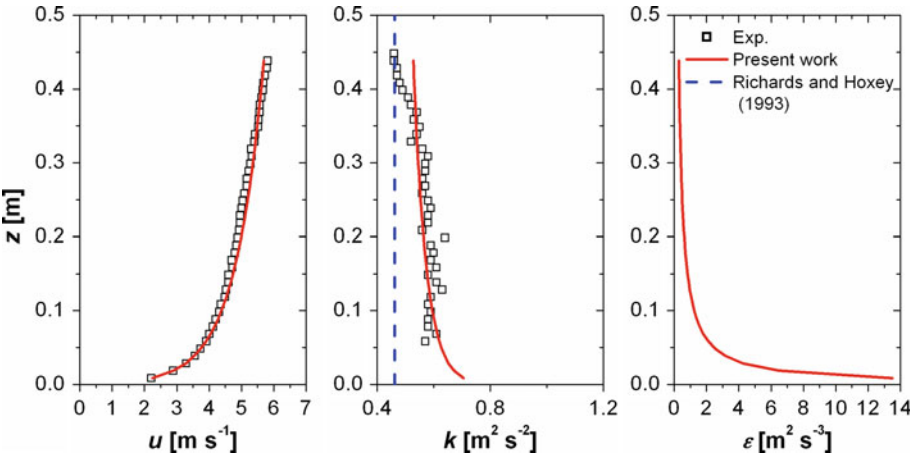

Fig. 2 Velocity, turbulent kinetic energy and turbulent dissipation rate inlet profiles

Table 2 Fitting parameters for velocity and turbulent kinetic energy inlet profiles

u_*	0.374 m s^{-1}
z_0	0.00075 m
C_1	−0.04
C_2	0.52

The computational grid (Fig. 1) was uniform in the longitudinal direction and stretched in the vertical direction to have the centre point of the inner cell adjacent to the wall at a height of 0.0025 m ($z^+ = 62.33$). The total number of cells was 28,400 (400×71 elements). Numerical simulations were carried out with the set of inlet conditions given by Eqs. (5), (7) and (15). The ABL parameters are listed in Table 2. As far as the boundary conditions are concerned, a pressure outlet condition was adopted at the outlet section, whereas the lower boundary was modelled with the rough-wall function described in Sect. 2.2. A constant strain was applied to the upper boundary, following the recommendation of Richards and Hoxey (1993).

3.2 Flow Around a Ground-Mounted Cube Immersed in a Wind-Tunnel Simulated Neutral ABL

The performances of the proposed approach for a non-homogeneous flow field were assessed simulating the flow around a single rectangular building, for which wind-tunnel data are available (CEDVAL A1-1, Leitl 1998). The geometry of the obstacle is shown in Fig. 3 and consists

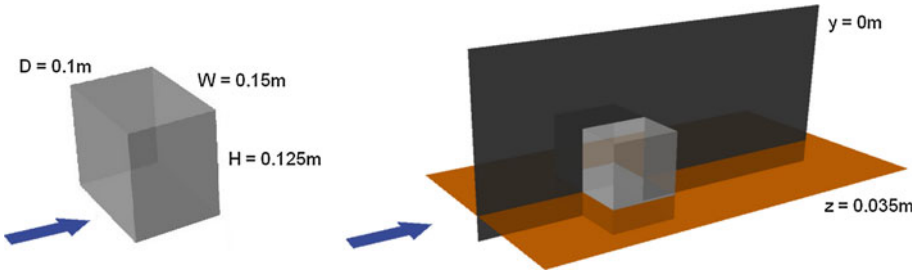

Fig. 3 Building geometry and location of measurement planes

of a ground-mounted rectangular shape with width 0.1 m, length 0.15 m and height 0.125 m. The inlet boundary of the computational domain was set 1 m upstream of the building, corresponding to the location where the ABL profiles were measured in the wind-tunnel; the outlet boundary was located 4 m downstream of the building. Being the model symmetrical with respect to the plane $y = 0$, only half of the domain was considered. The width and height of the domain were 0.65 and 1 m, respectively, equal to the wind-tunnel size.

The (half) building consisted of $20 \times 26 \times 40$ elements for a total number of cells of about 2.4 millions ($200 \times 114 \times 107$ elements). At the wall, the height of the ground adjacent cell was 0.00075 m. The new wall-function formulation allowed maintaining this resolution in the entire computational domain, as opposed to the simulations described in Gorlé et al. (2010). A grid sensitivity analysis was carried out to estimate the solution error associated to the discretization adopted. To this purpose, two additional grids were generated, with a uniform coarsening ratio, i.e. $r_h = h_i / h_1 = 1.15$ (Roache 1998) in the three directions, resulting in a total number of elements of about 1.74 and 1.26 millions, respectively. Following COST Action 732 (Franke et al. 2007), error estimates were obtained for the two variables of interest, i.e. velocity and turbulent kinetic energy, by comparing the results provided by the different grids at the locations where experimental data were available. The solution uncertainty, U_{sver}, was estimated following Logan and Nitta (2006), and the grid convergence index (GCI) was determined assuming a safety factor, $F_s = 1.25$, as advised by Roache (1998) for a set of three meshes. For the fine grid, a maximum GCI of 5 and 3% was determined for velocity and turbulent kinetic energy, respectively, by averaging the values obtained at all the measurement locations.

Numerical simulations were carried out with the same set of fully-developed conditions used for the homogenous ABL (Table 2). Concerning the other boundaries, a pressure outlet condition was applied at the outlet section and a symmetry condition was prescribed on the symmetry plane. A smooth-wall condition was imposed at the side and top boundaries and on the building wall, whereas the ground wall was modelled as a rough surface with $z_0 = 0.00075$ m. The use of the wall function described in Sect 2.2 allowed the automatic selection of the appropriate rough- or smooth-wall treatments.

Turbulence was modelled using the standard k–ε model with the Kato–Launder (KL) correction (Kato and Launder 1993) for the production term, to avoid the well-documented over-prediction of turbulent kinetic energy in the stagnation region (Lakehal and Rodi 1997; Murakami et al. 1997; Gorlé et al. 2010).

Three approaches were investigated for the definition of the parameter C_μ and of the source term S_ε. In a first case, Eq. (11) for C_μ and Eq. (8) for S_ε were applied within the entire computational domain, regardless of the building influence area (model denoted as undisturbed ABL—UABL). In a second case, a gradual transition of C_μ and S_ε was applied

Table 3 Summary of the investigated runs and model settings for the flow around a ground-mounted cube

Run	Model	Building influence area	ϕ (C_μ, S_ε)	α
1	UABL	–	ϕ_{hom}	–
2	ASL	Eq. (18)	Eq. (19)	$\frac{1}{2}$
3	ASQ			
4	PS	Half sphere	$\phi = \begin{cases} \phi_{\text{hom}} & \text{outside BIA} \\ \phi_{\text{std}} & \text{inside BIA} \end{cases}$	–

$S_{\varepsilon,\text{hom}}$ and $C_{\mu,\text{hom}}$, given by Eqs. (8) and (11); $C_{\mu,\text{std}} = 0.09$ and $S_{\varepsilon,\text{std}} = 0$

in the BIA, following the approach discussed in Sect. 2.3. Two different transition functions (Eq. 19) were tested, a linear ($\alpha = 1$) and a quadratic one ($\alpha = 2$). The corresponding models are indicated as automatic switch-linear (ASL) and automatic switch-quadratic (ASQ), respectively. Finally, following Gorlé et al. (2009), a last approach was considered, defining a priori the BIA (model denoted as prescribed switch—PS), as indicated in Sect. 2.3. For PS, C_μ and S_ε were set to 0.09 and 0, respectively, within the entire BIA, defined as a half sphere with radius 0.22 m and centre 0.02 m downstream of the building.

A summary of the performed simulations and model settings is shown in Table 3. Moreover, to visualize the difference between the investigated approaches, the variation of the model parameter C_μ according to the UABL, PS and ASQ models is shown in Fig. 4. The CFD results were compared to the experimental data for validation. Measurements are available for the symmetry plane ($y = 0$) and the horizontal plane $z = 0$ (Fig. 3). Experimental and numerical data were extracted and post-processed to obtain the contours of the non-dimensional velocity component, u/U_{ref}, and non-dimensional turbulent kinetic energy, k/U_{ref}^2, where U_{ref} is the longitudinal reference velocity, equal to 5.82 ms^{-1}. To quantify the agreement between measurements and numerical simulations, a hit rate q was defined for both velocity and turbulent kinetic energy as:

$$q = \frac{1}{N}\sum_{i=1}^{N} i_i \qquad i_i \begin{cases} 1 & \text{for } \left|\frac{V_{\text{CFD}} - V_{\text{TEST}}}{V_{\text{TEST}}}\right| \leq 0.25 \quad \text{or } |V_{\text{CFD}} - V_{\text{TEST}}| \leq W \\ 0 & \text{otherwise} \end{cases} \tag{20}$$

where $N$is the number of measurement positions, V_{CFD} and V_{TEST} represent the predicted and measured non-dimensional values. The hit rate indicates the fraction of N measurement points at which the CFD results are within 25% of the measurement data or within the uncertainty interval, W, of the data (Franke et al. 2007). The values used for W were 0.012 for u/U_{ref}, and 0.0316 $\left(k/U_{\text{ref}}^2\right)^{0.518}$ for k/U_{ref}^2 (Gorlé et al. 2010). Both the hit rate for all measurement points and local hit rates for selected regions (upstream, on the side, on top and downstream of the building) are presented in Table 4.

4 Results

4.1 Neutral ABL Over Flat Terrain

Figure 5 presents the evolution of the wall-shear stress in the longitudinal direction for the simulation of the neutral ABL described in Sect. 3.1. It can be observed how the proposed approach solves the typical issue related to the development of an internal boundary layer

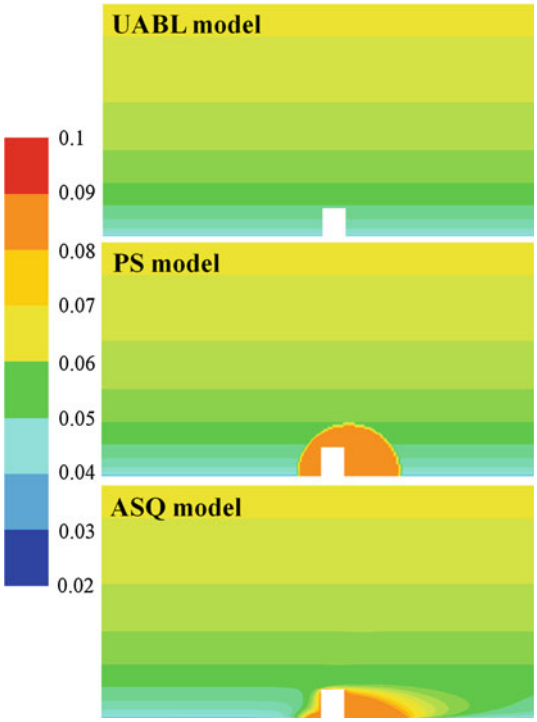

Fig. 4 Variation of the turbulence model parameter C_μ for the three modelling approaches ASL, ASQ and PS

Table 4 Hit-rate values for non-dimensional velocity and turbulent kinetic energy, varying the turbulence model setting

	Upstream	Side/top	Downstream	All
	u/U_{ref}			
Undisturbed ABL (UABL)	0.87	0.75	0.45	0.63
Automatic switch–linear (ASL)	0.87	0.75	0.49	0.65
Automatic switch–quadratic (ASQ)	0.85	0.77	0.45	0.62
Prescribed switch (PS)	0.86	0.82	0.57	0.70
	Upstream	Side/top	Downstream	All
	k/U_{ref}^2			
Undisturbed ABL (UABL)	0.60	0.51	0.65	0.61
Automatic switch–linear (ASL)	0.58	0.50	0.51	0.53
Automatic switch–quadratic (ASQ)	0.59	0.55	0.63	0.61
Prescribed switch (PS)	0.53	0.28	0.28	0.35

(Blocken et al. 2007a,b): the wall-shear stress remains uniform throughout the domain length after a short adaption length (of the order of 4% of the length of the computational domain). The uniformity of the wall-shear stress along the longitudinal direction is a first indication of the capability of the proposed approach to ensure homogeneity in the reproduction of the boundary layer. Figure 6a–c shows the comparison between inlet and outlet profiles of

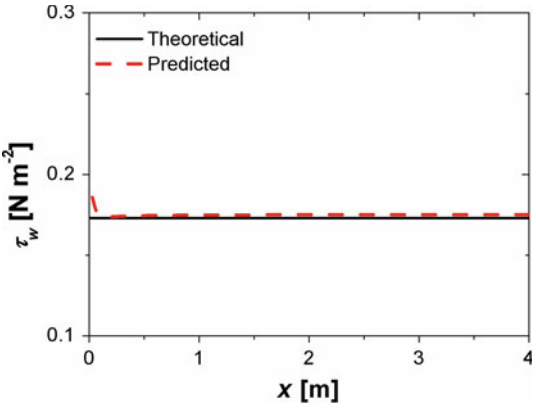

Fig. 5 Theoretical and predicted wall-shear stress as a function of the axial coordinate, obtained with the modified rough-wall function (Sect. 2.2)

velocity, turbulent kinetic energy and turbulent dissipation rate when Eqs. (5), (15) and (6) are specified at the inlet section of the domain. It can be observed how the overall modelling approach is able to ensure longitudinal and vertical homogeneity for the simulated boundary layer. The highest differences are observed for the k profile; however, these are below 2% in all cases. The results shown in Fig. 6a–c are further confirmed by Fig. 6d, which shows the non-dimensional velocity gradient $\Omega = (kz/u_*)\,(\partial u/\partial z)$. The latter allows the assessment of the deviation of the simulated velocity profile from the ideal logarithmic profile. Indeed, the Ω profile obtained at the outlet section of the domain closely follows the theoretical non-dimensional velocity gradient. It can be concluded that the set of boundary conditions defined by Eqs. (5), (15) and (6), the proposed modification to the standard k–ε model (Eqs. 8 and 11) and the rough-wall function formulation (Eq. 17) provide a comprehensive and consistent modelling approach for the neutral ABL.

4.2 Flow Around a Ground-Mounted Cube Immersed in a Wind-Tunnel Simulated Neutral ABL

Figures 7 and 8 present the contour plots for the non-dimensional velocity and turbulent kinetic energy, respectively, at planes $y = 0$ and $z = 0.035$ m. The experimental measurements are compared to the results obtained applying the UABL and ASQ models. Simulations were performed also with ASL and PS models (Sect. 3.2). However, only the ASQ results are shown in Figs. 7 and 8, as they provide the best compromise between the prediction of velocity and turbulent kinetic energy. On the other hand, a slower transition (ASL Model) was found to optimize the prediction of the velocity field and wake length, whereas turbulent kinetic energy was better reproduced when minimizing the building influence area. It can be observed (Fig. 7) that the application of the ABL model to the entire domain results in an over-prediction of the wake length by 85% with respect to the result provided by the measurements, i.e. 3.2H versus 1.7H. This is further confirmed by the contours of turbulent kinetic energy (Fig. 8), which show a large under-prediction of k downstream of the building. Therefore, the application of the UABL model within the full computational domain appears unsuited to properly reproduce the characteristics of the separation region, as indicated by former investigations (Gorlé et al. 2010).

When the ASQ model is applied, the wake length is decreased considerably, 2.6H, leading to an improved agreement with the test data; in particular, the deviation in the prediction of the bubble length is reduced from 85 to 46%. The ASQ model also provides a better

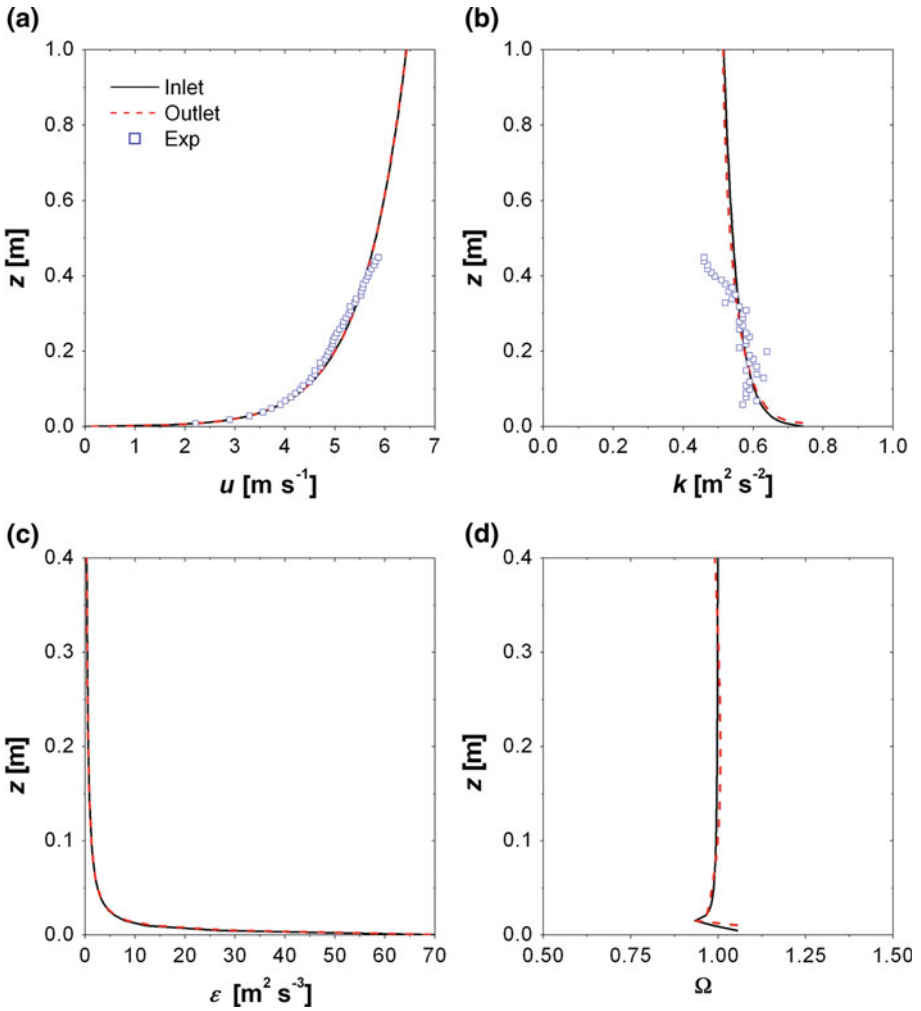

Fig. 6 Profiles of velocity (**a**), turbulent kinetic energy (**b**), turbulent dissipation rate (**c**) and non-dimensional velocity gradient (**d**) at inlet and outlet section of the computational domain, obtained with the proposed set on inlet conditions (Eqs. 5, 6 and 15) and the modified rough-wall function (Sect. 2.2)

reproduction of the turbulent kinetic energy field. The distribution of k on the planes $y = 0$ and $z = 0.035$ m shows that the proposed approach reduces the under-prediction of turbulent kinetic energy downstream of the building, leading to a better reproduction of the experimental field. However, the wake region is still over-predicted, thus indicating that the application of the automatic switch in the separation region can only alleviate the intrinsic limitations of the standard k–ε model for separated flows.

To allow a more quantitative comparison between experiments and numerical simulations, the calculated and measured non-dimensional vertical profiles of velocity and k are shown in Figs. 9 and 10, respectively, for different axial locations over and downstream of the building. Results were obtained applying the UABL, ASQ and PS models. It can be observed how the difference between the models becomes more pronounced downstream of the building,

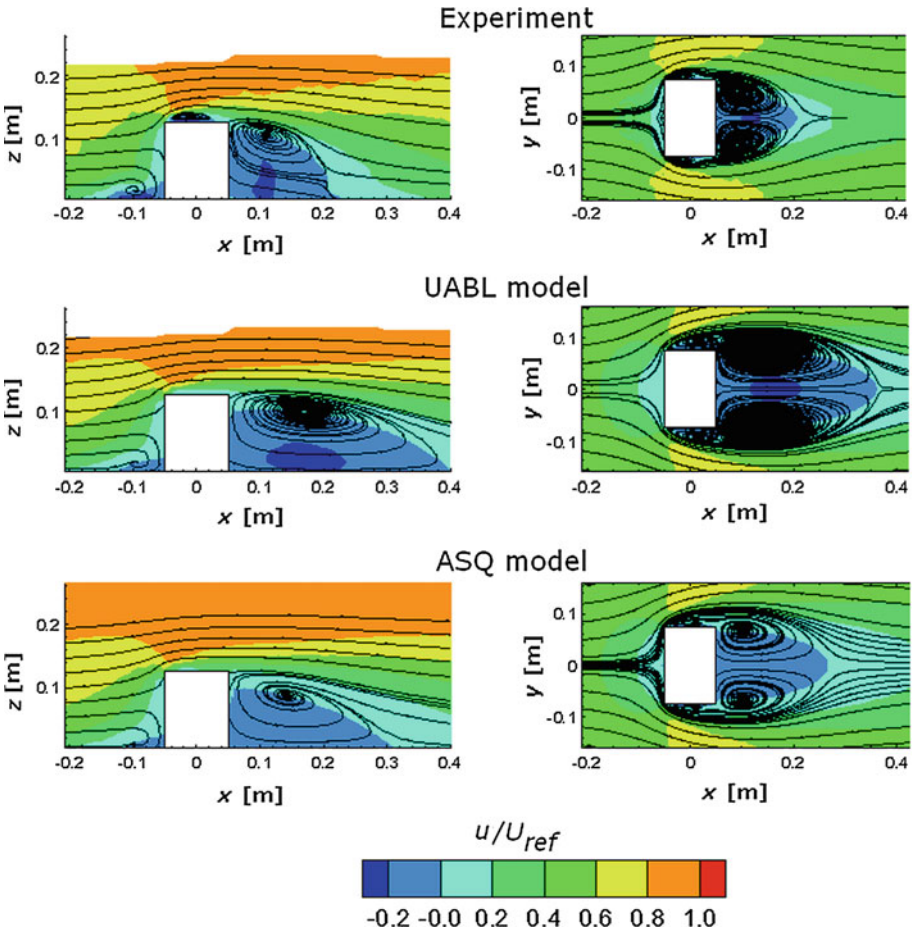

Fig. 7 Contour plots of non-dimensional velocity on the planes $y = 0$ (*left*) and $z = 0.035$ m (*right*)

in the wake region ($x = 0.105$ and 0.3 m). In particular, compared to the UABL model, ASQ allows the reduction of the under-prediction of velocity (Fig. 9) and the over-prediction of turbulent kinetic energy (Fig. 10) downstream of the building. It can also be remarked that the results obtained with ASQ are very similar to those provided by the PS model for the velocity distribution. On the other hand, the ASQ model performs better for turbulent kinetic energy (Fig. 10), particularly at location $x = 0.3$ m, where the PS model shows a strong over-prediction of k values. Nevertheless, the peak of k at $x = 0.105$ m is better captured by the PS model.

Finally, Table 4 lists the hit-rate values for the non-dimensional velocity and turbulent kinetic energy. For sake of clarity, all the investigated conditions are summarized in the Table. The first remark is that the hit rates obtained applying the UABL and ASQ models are very similar. In other words, it is not possible to distinguish which of the two model settings provides the best results by just comparing the hit-rate values. This is obviously due to the global nature of the hit-rate metric, which does not provide any information regarding the local prediction of flow features. To better clarify this aspect, Fig. 11 shows the local hits

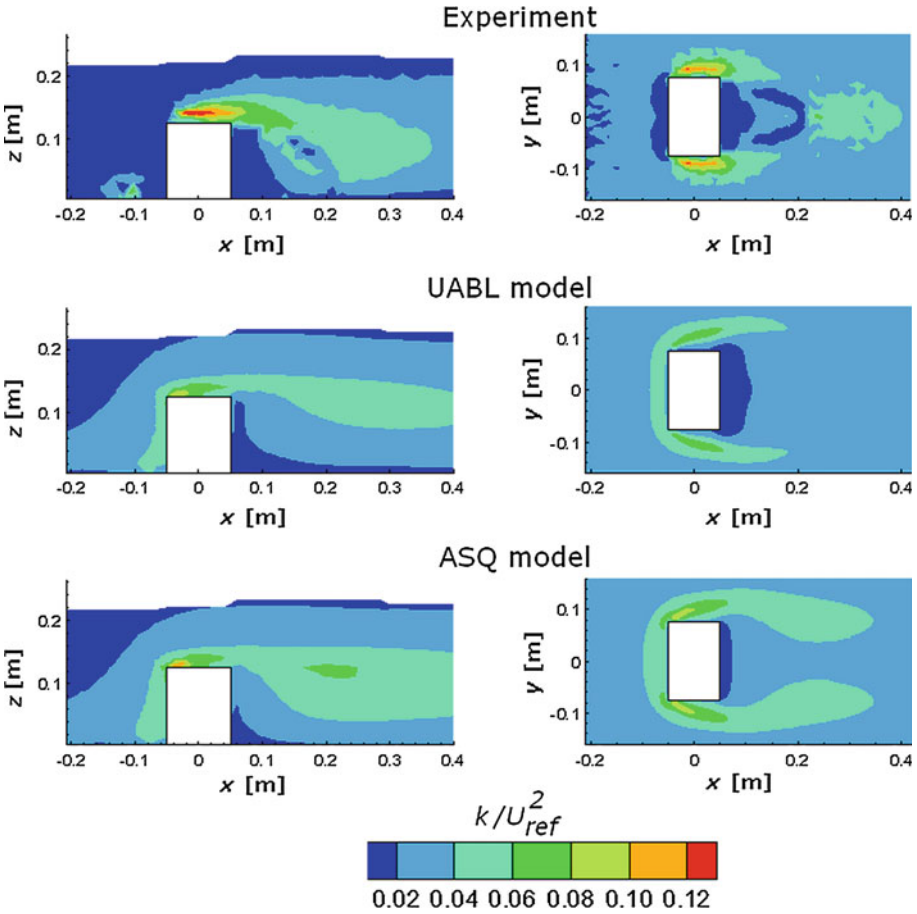

Fig. 8 Contour plots of non-dimensional turbulence kinetic energy on the planes $y = 0$ (*left*) and $z = 0.035$ m (*right*)

for the turbulent kinetic energy field, obtained applying the ASQ and UABL models, respectively. It is clear that ASQ provides better results in the wake, as confirmed by the increased number of hits. However, the global hit-rate values for the two cases are very similar due to the poorer performances of the ASQ model at the border of the wake, where the turbulent kinetic energy is over-estimated, as indicated by the contour plots in Fig. 8. As far as the other approaches are concerned, both the ASL and the PS models optimize the reproduction of the velocity field, but significantly penalize the prediction of turbulent kinetic energy.

To conclude, the ASQ model can be regarded as the best performing option for the present investigation. In particular, it ensures the best compromise between the prediction of velocity and turbulent kinetic energy in the BIA, providing hit-rate values higher than 60% for both fields. This represents a slight but non-negligible improvement with respect to the results given by Gorlé et al. (2010) and Parente et al. (2011). Indeed, significant developments are still needed to attain fully satisfactory results. In particular, future study will investigate the possibility of adapting the proposed formulation to more complex turbulence models, such as the Reynolds stress model, to avoid the intrinsic limitations of standard k–ε in the wake

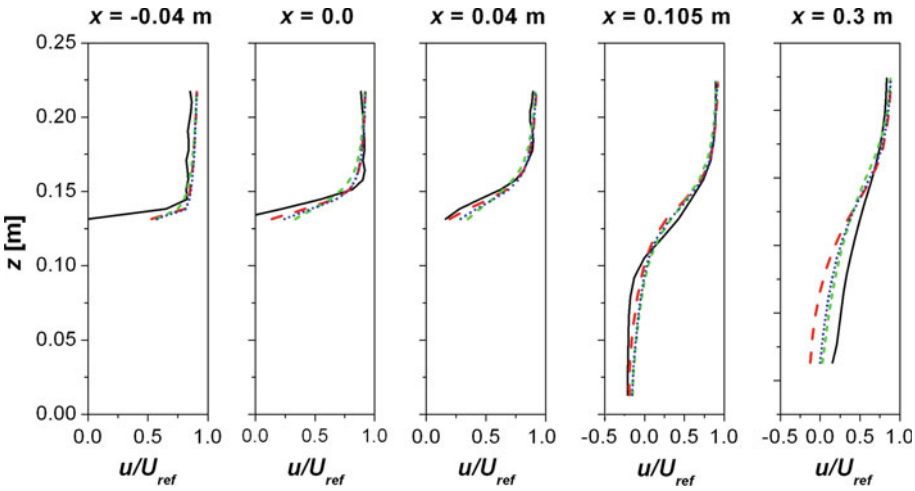

Fig. 9 Experimental and numerical profiles of non-dimensional velocity over and downstream of the obstacle. *Solid line* experimental data. *Dashes* UABL model. *Short dashes* PS model. *Dots* ASQ model

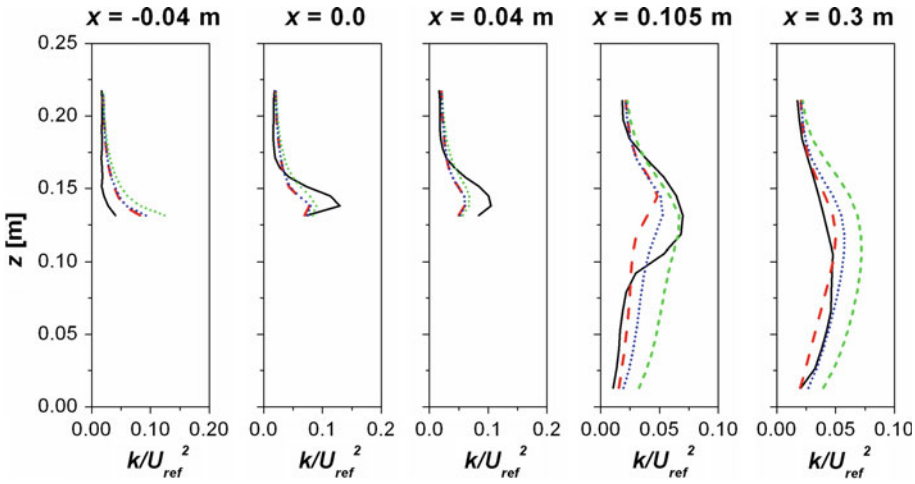

Fig. 10 Experimental and numerical profiles of non-dimensional turbulent kinetic energy over and downstream of the obstacle. *Solid line* experimental data. *Dashes* UABL model. *Short dashes* PS model. *Dots* ASQ model

region. As a matter of fact, other variants of the k–ε model were tested within the present study, to improve the predictions in the wake. In particular, the MMK model proposed by Murakami et al. (1997) appeared as the most promising, due to the dependency of the parameter C_μ on the vorticity/strain-rate ratio. However, the results of the MMK model with a quadratic blending function (ASQ-MMK) lead to a hit rate for velocity comparable to that provided by ASQ (0.64 vs. 0.61), but to a much lower hit rate for turbulent kinetic energy (0.5 vs. 0.61).

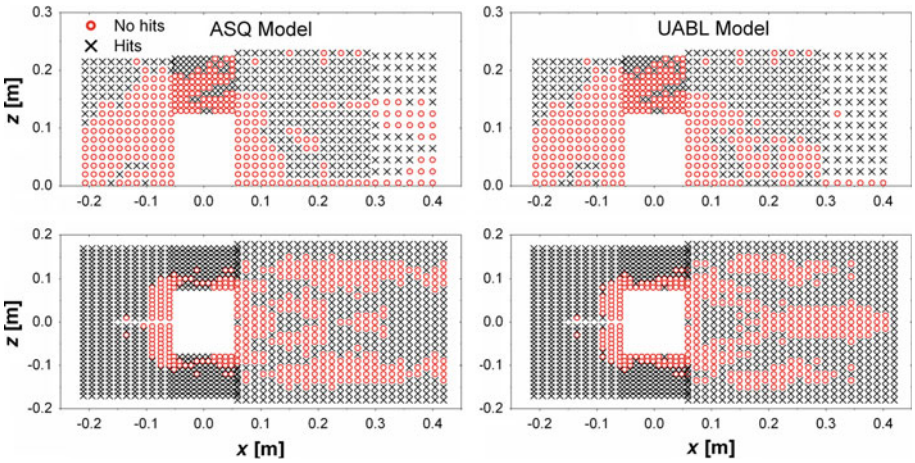

Fig. 11 Local hit rates for the non-dimensional turbulent kinetic energy, applying the ASQ model (*left*) and the UABL model (*right*)

5 Conclusions

A comprehensive approach to the numerical simulation of the neutral ABL with the standard k–ε turbulence model was presented. A new inlet profile for turbulent kinetic energy was determined from the solution of the turbulent kinetic energy transport equation. Consistency between the inlet profiles and the turbulence model was accomplished through the re-definition of the turbulence model parameter C_μ and the introduction of a source term, S_ε, in the turbulent dissipation rate transport equation. The modelling approach was completed by a wall function, including both the classic treatment for smooth-walls and a rough-wall formulation based on the aerodynamic roughness, to ensure full consistency with the inlet conditions.

The proposed methodology was first validated for a neutral ABL over flat terrain. Results showed the capability of the proposed approach of ensuring the desired homogeneity of velocity and turbulent quantities throughout the computational domain. Subsequently, the flow around a ground-mounted bluff body was simulated, to investigate the applicability of the approach to cases involving obstacles immersed in the ABL. To this purpose, a novel algorithm was proposed to identify the building influence area and modify the turbulence model. Results indicated a non-negligible improvement with respect to previous investigations, especially in the prediction of turbulent kinetic energy. Future study will focus on the extension of the proposed methodology to different turbulence models, i.e. the Reynolds stress model, to overcome the intrinsic weakness of the k–ε model in the simulation of separated flows.

Acknowledgments We would like to thank the reviewers for valuable comments and suggestions, and also express our gratitude to the group of Prof. Leitl at the University of Hamburg, for making high-fidelity experimental data available. The second author's contribution to this study while at the University of Antwerp was supported by IWT Vlaanderen, the Institute for the Promotion of Innovation by Science and Technology in Flanders, through the SBO project NanoSoc.

References

Beranek W (1979) General rules for the determination of wind environment. In: Proceedings of the 5th international conference on wind engineering, Fort Collins, Colorado, USA, pp 225–234

Blocken B, Carmeliet J, Stathopoulos T (2007a) CFD evaluation of wind speed conditions in passages between parallel buildings—effect of wall-function roughness modifications for the atmospheric boundary layer flow. J Wind Eng Ind Aerodyn 95:941–962

Blocken B, Stathopoulos T, Carmeliet J (2007b) CFD simulation of the atmospheric boundary layer: wall function problems. Atmos Environ 41:238–252

Cebeci T, Bradshaw P (1977) Momentum transfer in boundary layers. Hemisphere Publishing Corporation, New York, 416 pp

Dejoan A, Santiago JL, Martilli A, Martin F, Pinelli A (2010) Comparison between LES and RANS computations for the MUST field experiment. Part II: Effects of incident wind angle deviation on the mean flow and plume dispersion. Boundary-Layer Meteorol 135:133–150

Franke J, Hirsch C, Jensen A, Krus H, Schatzmann M, Westbury P, Miles S, Wisse J, Wright N (2004) Recommendations on the use of CFD in wind engineering. In: COST Action C14, Impact of wind and storm on city life built environment, von Karman Institute, pp C1.1–C1.11

Franke J, Hellsten A, Schlunzen H, Carissimo B (eds) (2007) Best practice guideline for the CFD simulation of flows in the urban environment—COST Action 732. COST office, 52 pp

Gorlé C, Beeck Jvan , Rambaud P, Tendeloo Gvan (2009) CFD modelling of small particle dispersion: the influence of the turbulence kinetic energy in the atmospheric boundary layer. Atmos Environ 43:673–681

Gorlé C, Beeck Jvan , Rambaud P (2010) Dispersion in the wake of a rectangular building: validation of two RANS modelling approaches. Boundary-Layer Meteorol 137:115–133

Hargreaves D, Wright N (2007) On the use of the k–ε model in commercial CFD software to model the neutral atmospheric boundary layer. J Wind Eng Ind Aerodyn 95:355–369

Kato M, Launder B (1993) The modeling of turbulent flow around stationary and vibrating square cylinders. In: Proceedings of 9th symposium on turbulence and shear flows, Kyoto, Japan, pp 1–6

Lakehal D, Rodi W (1997) Calculation of the flow past a surface-mounted cube with two-layer turbulence models. J Wind Eng Ind Aerodyn 67&68:65–78

Leitl B (1998) Cedval at Hamburg University. http://www.mi.uni-hamburg.de/cedval

Lim H, Thomas T, Castro I (2009) Flow around a cube in a turbulent boundary layer: LES and experiment. J Wind Eng Ind Aerodyn 97:96–109

Logan RW, Nitta CK (2006) Comparing 10 methods for solution verification, and linking to model validation. J Aero Comput Inform Commun 3:354–373

Murakami S, Mochida A, Kondo K, Ishida Y, Tsuchiya T (1997) Development of a new k-ε model for flow and pressure fields around bluff body. J Wind Eng Ind Aerodyn. 67(68):169–182

Nikuradse J (1933) Stromungsgesetze in rauhen Rohren. Forschung Arb. Ing.-Wes. No. 361

Norris SE, Richards PJ (2010) Appropriate boundary conditions for computational wind engineering models revisited. In: Proceedings of the Fifth International Symposium on Computational Wind Engineering (CWE2010) Chapel Hill, North Carolina, USA, May 23–27, pp 1–8

Parente A., Benocci C (2010) On the RANS simulation of neutral ABL flows, In: Proceedings of the Fifth International Symposium on Computational Wind Engineering (CWE2010) Chapel Hill, North Carolina, USA, May 23–27, pp 1–8

Parente A, Gorlé C, Beeck Jvan , Benocci C (2011) Improved k–ε model and wall function formulation for the RANS simulation of ABL flows. J Wind Eng Ind Aerodyn 99:267–278

Pontiggia M, Derudi M, Rota R (2009) Hazardous gas dispersion: a CFD model accounting for atmospheric stability classes. J Hazard Mater 171:739–747

Richards P, Hoxey R (1993) Appropriate boundary conditions for computational wind engineering models using the k–ε turbulence model. J Wind Eng Ind Aerodyn 46(47):145–153

Riddle A, Carruthers D, Sharpe A, McHugh C, Stocker J (2004) Comparisons between FLUENT and ADMS for atmospheric dispersion modelling. Atmos Environ 38:1029–1038

Roache PJ (1998) Verification and validation in computational science and engineering. Hermosa Publishers, Albuquerque, NM, 464 pp

Rodi W (1997) Comparison of LES and RANS calculations of the flow around bluff bodies. J Wind Eng Ind Aerodyn 69–71:55–75

Shah K, Ferziger J (1997) A fluid mechanicians view of wind engineering: large eddy simulation of flow past a cubic obstacle. J Wind Eng Ind Aerodyn 67&68:211–224

Xie Z, Castro IP (2006) LES and RANS for turbulent flow over arrays of wall-mounted obstacles. Flow Turbul Combust 76:291–312

Xie Z, Voke PR, Hayden P, Robins AG (2004) Large-eddy simulation of turbulent flow over a rough surface. Boundary-Layer Meteorol 111:417–440

Yang Y, Gu M, Chen S, Jin X, Jin H, Gu M, Chen S (2009) New inflow boundary conditions for modelling the neutral equilibrium atmospheric boundary layer in computational wind engineering. J Wind Eng Ind Aerodyn 97:88–95